ISSN 0021-3640, JETP Letters, 2009, Vol. 90, No. 6, pp. 433–437. © Pleiades Publishing, Ltd., 2009.
Original Russian Text © M.R. Shcherbakov, P.P. Vabishchevich, M.I. Dobynde, T.V. Dolgova, A.S. Sigov, C.M. Wang, D.P. Tsai, A.A. Fedyanin, 2009, published in Pis'ma v Zhurnal Éksperimental'noĭ i Teoreticheskoĭ Fiziki, 2009, Vol. 90, No. 6, pp. 478–482.

Plasmonic Enhancement of Linear Birefringence and Linear Dichroism in Anisotropic Optical Metamaterials¶

M. R. Shcherbakov[a], P. P. Vabishchevich[a], M. I. Dobynde[a], T. V. Dolgova[a], A. S. Sigov[b], C. M. Wang[c], D. P. Tsai[c], and A. A. Fedyanin[a]

[a] *Moscow State University, Moscow, 119991 Russia*

e-mail: shcherbakov@nanolab.phys.msu.ru, fedyanin@nanolab.phys.msu.ru

[b] *Moscow State Institute of Radioengineering, Electronics, and Automation, Moscow, 119454 Russia*

[c] *Department of Physics, National Taiwan University, 10617 Taipei, Taiwan, Republic of China*

Received July 31, 2009

The resonant behavior of linear birefringence and linear dichroism spectra is found in anisotropic optical metamaterials made of noble metal thin films with stripes and rectangular hole nanoapertures forming one- or two-dimensional subwavelength gratings. Differences in effective refractive index and extinction coefficient for linearly polarized eigenstates are increased in spectral range of resonances of local and surface plasmon-polaritons at the normal incidence and reach the values of $\Delta n \simeq 2.5$ and $\Delta\kappa \simeq 2.75$, respectively.

PACS numbers: 67.70.Qs, 73.20.Mf, 77.22.Ej

DOI: 10.1134/S0021364009180064

Development of nanofabrication technology has led to a vast variety of new tasks concerning optical effects in metamaterials. Optical metamaterials are produced from bulk media or thin films by lithographic methods which imply spatial structuring on the scale of tens of nanometers. This gives rise to optical properties absent in the initial material. Negative refractive index [1, 2], spatial localization of light in complex planar waveguides based on plasmonic crystals [3], optical resolution exceeding the diffraction limit [4, 5] were observed recently in optical metamaterials. Noble metals are a common basis for the most of the optical metamaterials and these effects are usually being associated with excitation of surface plasmon-polaritons (SPP) at metal-dielectric interfaces. Planar metamaterials based on thin metal films are significantly easier to manufacture than three-dimensional ones and they also manifest resonant optical response leading to various effects in optical range. If a periodic array of subwavelength holes is created in a metal film with thickness of several skin layers, the effect of extraordinary optical transmission is observed—the transmitted electromagnetic wave intensity is drastically enhanced at surface plasmon resonance wavelength with comparison to off-resonance frequencies [6]. The intensity of such a wave can reach tens of percent of the incident-wave intensity.

Metamaterials with anisotropic nanostructuring such as arrays of rectangular nanoholes [7], elliptical holes [8] or holes of a more complex shape [9] are capable of changing the polarization state of transmitted or reflected light. For example, strong influence of the shape of nanoholes on the transmission spectrum of linearly polarized light was observed [7, 10]. The measurement of the Stokes parameters of light transmitted through the anisotropic metamaterial indicates a high phase delay introduced to one of the polarization eigenmodes of the metamaterial [11]. However, the role of local and surface plasmon-polaritons in mechanisms of optical anisotropy of metamaterials has not been established yet since it requires the study of polarization conversion in a broad spectral range.

In this paper mechanisms of resonant enhancement of polarization effects—linear birefringence and linear dichroism—are systematically studied in anisotropic planar optical metamaterials made of submicron noble metal films. The role of plasmon excitations in polarization conversion by anisotropic metamaterials is clarified.

Samples of anisotropic metamaterials were fabricated from thin silver and gold films thermally evaporated onto fused silica substrates. Sample 1 was a silver film of 150 nm thickness with an array of rectangular apertures made by ion-beam lithography. Holes of 100×300 nm size formed a square lattice with a period of 400 nm (Fig. 1a), the size of nanostructured area was 100×100 μm. Sample 2 was fabricated using electron beam lithography and consisted of array of gold stripes 130 nm in width and 30 nm in thickness with a period of 330 nm. Total size of nanostructured area was 30×30 μm (Fig. 1b). Both samples possessed the second-order rotational symmetry with axis perpen-

¶The article was translated by the authors.

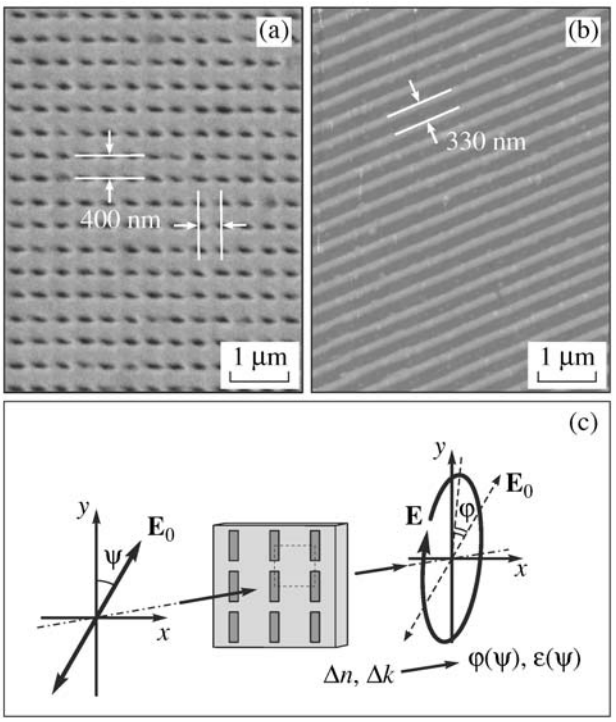

Fig. 1. (a) Scanning electron microscope image of silver film perforated with array of rectangular apertures (sample 1). The apertures have lateral size of 100 × 300 nm and are packed in a square lattice with 400 nm period. (b) Atomic force microscope image of the golden stripes array (sample 2). The array has a period of 330 nm with stripe width of 130 nm. (c) Schematic of polarization conversion in anisotropic metamaterial.

dicular to the plane of the sample. As linearly polarized light passes through an anisotropic metamaterial it becomes elliptically polarized with the ratio of axes $\mathscr{E}$. Major axis of the ellipse is rotated by angle φ relative to the direction of the polarization of the incident light as is schematically shown in Fig. 1c. Such polarization conversion corresponds to an anisotropic absorptive medium with differences in effective refractive index Δn and extinction coefficient $\Delta\kappa$ for ordinary and extraordinary rays.

Parameters of visible light transmitted through the samples of metamaterials were determined by microspectroscopy of transmission coefficient. The setup is capable of measurement of linearly polarized light transmission spectra providing signal detection from a sample area of 30 × 30 μm with the control of the rotation and ellipticity of transmitted light polarization in the wavelength range from 400 to 750 nm with an accuracy of 0.5°.

Figure 2 shows transmission spectra of anisotropic metamaterial samples for different orientations of the incident radiation polarization obtained without analyzer. Spectra *1* and *3* correspond to the polarization of incident light along the stripes and along the major

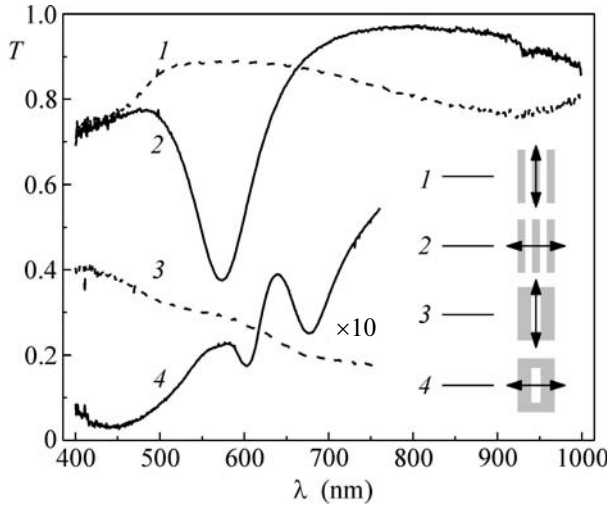

Fig. 2. Linearly polarized light transmission spectra of anisotropic metamaterials at normal incidence. The inset shows the geometry of the experiment, where the arrows indicate the polarization orientation.

axis of rectangular nanoholes, respectively, and do not contain any resonances in the visible and near-IR bands. Spectrum *2* obtained for polarization orthogonal to the stripes of sample 2 demonstrates a resonance at $\lambda \simeq 585$ nm with a width of 80 nm. The ratio of transmission coefficients for orthogonal linear polarized states at this wavelength is approximately 2.4. Spectra *1* and *2* intersect at $\lambda \simeq 670$ nm indicating the absence of linear dichroism at this wavelength. Spectrum *4* obtained for the orientation of light polarization parallel to the minor axis of rectangular nanoholes increases with wavelength and has two local maxima of transmittance at wavelengths of 580 nm and 640 nm. Spectra *3* and *4* intersect at $\lambda \simeq 620$ nm providing zero linear dichroism.

Optical response of sample 2 can be considered as polarization-sensitive response of long nanorods with elliptical cross-section. The polarizability of a single rod with subwavelength cross-section is given as $\alpha \propto (L(\varepsilon(\lambda) - \varepsilon_0) + \varepsilon_0)^{-1}$, where the polarization is oriented along the major axis of the cross-section, ε stands for rod material permittivity, ε_0 stands for surrounding medium permittivity and L is a form-factor, which depends on geometrical parameters of rod cross-section [12]. For axes ratio of 30 nm : 130 nm one can get $L \simeq 0.19$ and $\alpha \propto (\varepsilon(\lambda) + 4.3\varepsilon_0)^{-1}$. As $\varepsilon(\lambda) \simeq -4.3\varepsilon_0$ resonant response of the rod and extinction enhancement related to local plasmon resonance are observed. Variation of ε_0 from 1 (air) to 2.4 (quartz substrate) results in spectral shift of resonant wavelength from 520 nm to 660 nm that explains the extinction maximum spectral position in Fig. 2. Such resonance is absent for orthogonal polarization state because local plasmons are weakly excited.

Peculiarities observed in transmission spectra of sample 1 are caused by excitation of SPP modes of different nature. As light is diffracted along the surface of the grating SPPs are excited at metal-dielectric interface. In this case the wavelength of SPP resonance excitation is given as

$$\lambda_{(i,j)} = \frac{2\pi}{a_0}\frac{1}{\sqrt{i^2+j^2}}\sqrt{\frac{\varepsilon\varepsilon_0}{\varepsilon+\varepsilon_0}}, \quad (1)$$

where ε and ε_0 are the permittivities of metal and dielectric surrounding, respectively, i and j are integers and a_0 is grating period [6]. For sample 1 resonances with low values of i and j exist in visible and UV regions at $\lambda^q_{(1,0)} = 525$ nm, $\lambda^a_{(1,0)} = 440$ nm, and $\lambda^q_{(1,1)} = 415$ nm and $\lambda^a_{(1,1)} = 365$ nm (indices q and a correspond to silver-quartz and silver-air interfaces, respectively). Resonant wavelength depends strongly on the hole configuration, namely, the increase of axes ratio causes the redshift of resonances [13]. The reason for such a shift is existence of another type of plasmonic modes in metamaterials, so-called localized plasmonic modes [14]. The energy of a localized mode is concentrated inside aperture and transferred from SPPs scattered by the aperture. The wavelength of the first localized mode represents the cut-off wavelength λ_c of the aperture and it is the longest wavelength which light can possess to effectively pass through the hole. The wavelength λ_c is redshifted if the shape of the aperture is changed from square to rectangular one [15]. The cut-off wavelength for sample 1 is located in IR region and equals to $\lambda_c \simeq 890$ nm for light polarized perpendicular to the major axis of the hole. The combination of propagating and localized SPP excitations defines the following picture of the transmission spectrum: the (1, 0) q-maximum is redshifted into the near-IR region, while all other maxima are shifted into the visible. The cut-off wavelength for the light with orthogonal polarization state is $\lambda_c \simeq 390$ nm which explains the monotonic decay of the transmittance spectrum with the increase of the wavelength.

Output polarization state parameters such as ellipticity $\mathscr{E}(\psi)$ and rotation angle $\varphi(\psi)$ were measured as functions of the azimuth angle ψ for determination of birefringence and dichroism. Typical dependences for samples 1 and 2 are presented in Fig. 3 for wavelengths of 640 nm and 585 nm which are central wavelengths of resonant peculiarities for samples 1 and 2, respectively.

Depolarization of transmitted light was defined for sample 1 at $\lambda = 625$ nm by placing a quarter-wave plate in front of the analyzer in such a way that the variation of light intensity I coming out from analyzer was maximal on the full range of the analyzer angle. Ratio $I_{\min}/I_{\max}$ is defined to be approximately 0.2 $\mathscr{E}^2$ for every ψ value. Depolarization is most likely caused by the high value of numerical aperture of the illuminating system which causes the presence of different spatial Fourier-harmonics in incident light beam having different polarization-sensitive cross-sections [16].

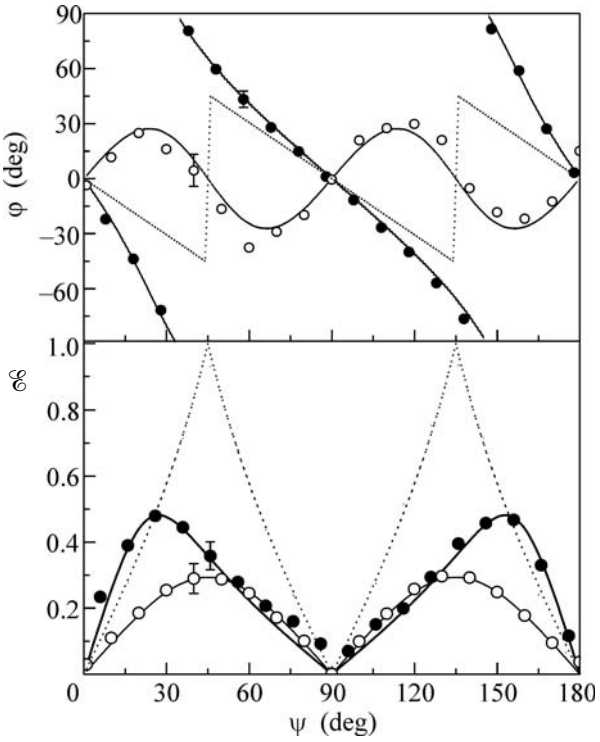

Fig. 3. (Top) The rotation angle φ of the polarization ellipse and (bottom) the ellipticity $\mathscr{E}$ of light transmitted through anisotropic optical metamaterial samples versus the azimuth angle ψ. Experimental data are shown (open circles) for sample 1 at $\lambda = 640$ nm and (closed circles) for sample 2 at $\lambda = 585$ nm. The solid curves show the fit of the experimental data with Eq. (6) with $\Delta n + \imath\Delta\kappa = 1.3 + 0.6\imath$ and $\Delta n + \imath\Delta\kappa = 1.4 + 2.7\imath$. For comparison, the dependences $\varphi(\psi)$ and $\mathscr{E}(\psi)$ for the quarter-wave plate are shown by the dotted lines.

The $\mathscr{E}(\psi)$ and $\varphi(\psi)$ dependences demonstrate presence of two incident light polarization states with $\psi = 0°$, 90° which are conserved upon propagation through the samples. These directions correspond to E-field parallel and perpendicular to the optical axes of the metamaterials. Taking the Oy axis coincides with the optical axis as is shown in Fig. 1c, normalized initial polarization state vector can be written as

$$\mathbf{P}_0 = \begin{pmatrix} \sin\psi \\ \cos\psi \end{pmatrix}. \quad (2)$$

The linear birefringence of the medium causes the phase delay $\Delta\phi$ between the E_x and E_y components of the electric field $\mathbf{E}$ proportional to the refractive index difference $n_y - n_x$. Linear dichroism of the medium changing the E_x/E_y relation and is characterized by $\Delta\chi$ proportional to the extinction coefficient difference.

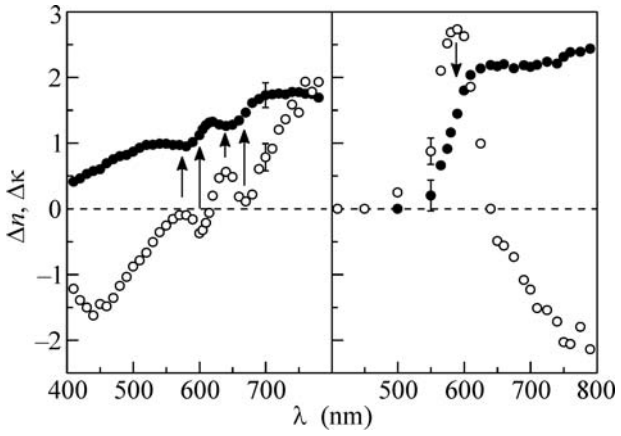

Fig. 4. Spectra of complex birefringence (closed circles) Δn and (open circles) $\Delta\kappa$ for samples (left) 1 and (right) 2. The arrows indicate the maxima and minima of $\Delta\kappa$ dependences and corresponding inflection points of Δn dependences.

The output polarization state vector is written as follows:

$$\mathbf{P} = K\begin{pmatrix} \sin\psi\, e^{\imath\Delta\phi - \Delta\chi} \\ \cos\psi \end{pmatrix}, \quad (3)$$

where

$$\Delta\phi = \frac{2\pi d}{\lambda}\Delta n, \quad \Delta\chi = \frac{2\pi d}{\lambda}\Delta\kappa, \quad (4)$$

K is a constant accounting for absorption and reflection and it does not affect the polarization state and d is metamaterial thickness. Polarization vector circumscribes an ellipse whose E-field absolute value is described by the following expressions:

$$|E(t)| = \sqrt{E_x^2(t) + E_y^2(t)} = \sqrt{e^{-2\Delta\chi}\sin^2\psi\cos^2(\Delta\phi + t) + \cos^2\psi\cos^2 t}. \quad (5)$$

Light ellipticity and polarization plane rotation are equal to

$$\mathscr{E}(\psi) = \frac{|E_{\min}|}{|E_{\max}|},$$

$$\varphi(\psi) = \arctan\frac{\mathrm{Re}\,E_x(t_{\max})}{\mathrm{Re}\,E_y(t_{\max})} - \psi = \arctan\left(e^{-\Delta\chi}\tan\psi\frac{\cos(\Delta\phi + t_{\max})}{\cos t_{\max}}\right) - \psi, \quad (6)$$

where $|E_{\min}|$ and $|E_{\max}|$ are minimal and maximal values of electric field in Eq. (5), $t_{\max}$ stands for the time moment at which the absolute value of the E-field reaches its maximum. Birefringence and dichroism magnitudes are defined by fitting the experimental dependences $\mathscr{E}(\psi)$ and $\varphi(\psi)$ by Eq. (6). Figure 3 shows fitting curves obtained for $\Delta n + \imath\Delta\kappa = 1.3 + 0.6\imath$ at $\lambda = 640$ nm for sample 1 and $\Delta n + \imath\Delta\kappa = 1.4 + 2.75\imath$ at $\lambda = 585$ nm for sample 2.

Figure 4 shows dependences $\Delta n(\lambda)$ and $\Delta\kappa(\lambda)$ for both anisotropic metamaterial samples. $\Delta n(\lambda)$ and $\Delta\kappa(\lambda)$ dependences indicate dichroism maximum as well as the birefringence increase for sample 2 in the vicinity of local plasmon resonance at $\lambda \simeq 585$ nm. $\Delta n(\lambda)$ turns to zero at $\lambda \simeq 640$ nm corresponding to the intersection of linear polarized light transmission spectra in Fig. 2 while Δn gets saturated and changes weakly over near-IR range. Birefringence is absent in the region of $\lambda \lesssim 520$ nm where plasmon propagation length is less than a wavelength of light. This determines the importance of a plasmonic excitation in optical anisotropy of the metamaterial. Similar dependences are observed for sample 1: maxima and minima of $\Delta\kappa(\lambda)$ dependence coincide with inflection points of $\Delta n(\lambda)$ dependence.

Refractive index difference reaches the value of $\Delta n \simeq 2.5$ for sample 2 that is about an order of magnitude larger than that for conventional bulk anisotropic media such as BBO crystal with $\Delta n \simeq 0.12$ in the visible. The phase shift introduced by metamaterial with rectangular holes reaches the value of 0.7π at $\lambda \simeq 700$ nm that corresponds to the value of $\Delta n \simeq 1.65$. Such a large phase delay is most likely provided by low group velocity of SPPs in one of the polarization modes [17]. The phase delay exceeds that of anisotropic nanoparticle arrays by approximately 4 times [18].

In conclusion, plasmonic enhancement of linear birefringence and dichroism is observed in anisotropic optical metamaterials made of nanostructured silver and gold films. Experimental spectra of refractive index and extinction coefficient differences for ordinary and extraordinary rays demonstrate the enhancement of linear birefringence and dichroism up to $\Delta n \simeq 2.5$ and $\Delta\kappa \simeq 2.75$ in the vicinity of local and propagating surface plasmon resonances. Large phase delays and polarization-sensitive transmission at submicron thicknesses allow the effective control of the polarization state of light at the subwavelength scale by anisotropic plasmonic metamaterials.

This work was supported by the Russian Foundation for Basic Research and the Federal Agency for Education.

REFERENCES

1. V. G. Veselago, Sov. Phys. Usp. **10**, 509 (1968).
2. R. A. Shelby, D. R. Smith, and S. Schultz, Science **292**, 77 (2001).
3. I. Bozhevolnyi, J. Erland, K. Leosson, et al., Phys. Rev. Lett. **86**, 3008 (2001).
4. F. M. Huang and N. I. Zheludev, Nano Lett. **9**, 1249 (2009).
5. J. B. Pendry, Phys. Rev. Lett. **85**, 3966 (2000).

6. T. W. Ebbesen, H. J. Lezec, H. F. Ghaemi, et al., Nature **391**, 667 (1998).
7. K. J. Klein Koerkamp, S. Enoch, F. B. Segerink, et al., Phys. Rev. Lett. **92**, 183901 (2004).
8. J. Elliott, I. I. Smolyaninov, N. I. Zheludev, et al., Opt. Lett. **29**, 1414 (2004).
9. T. Li, H. Liu, S. Wang, et al., Appl. Phys. Lett. **93**, 021110 (2008).
10. R. Gordon, A. G. Brolo, A. McKinnon, et al., Phys. Rev. Lett. **92**, 037401 (2004).
11. X.-F. Ren, P. Zhang, G.-P. Guo, et al., Appl. Phys. B **91**, 601 (2008).
12. H. C. van de Hulst, *Light Scattering by Small Particles* (Dover, New York, 1981).
13. K. L. van der Molen, K. J. Klein Koerkamp, and S. Enoch, Phys. Rev. B **72**, 045421 (2005).
14. A. Degiron and T. W. Ebbesen, J. Opt. A: Pure Appl. Opt. **7**, S90 (2005).
15. R. Gordon and A. G. Brolo, Opt. Express **13**, 1933 (2005).
16. E. Altewischer, C. Genet, M. P. Van Exter, et al., Opt. Lett. **30**, 90 (2005).
17. V. V. Temnov, U. Woggon, J. Dintinger, et al., Opt. Lett. **32**, 1235 (2007).
18. J. Sung, M. Sukharev, E. M. Hicks, et al., J. Phys. Chem. C **112**, 3252 (2008).